 CMES, vol.66, no.3, pp.227-248, 2010

A Time-Domain Meshless Local Petrov-Galerkin Formulation for the Dynamic Analysis of Nonlinear Porous Media

Delfim Soares Jr.[1]

Abstract: In this work, a meshless method based on the local Petrov–Galerkin approach is proposed for the solution of pore-dynamic problems considering elastic and elastoplastic materials. Formulations adopting the Heaviside step function as the test functions in the local weak form are considered. The moving least-square method is used for the approximation of physical quantities in the local integral equations. After spatial discretization is carried out, a nonlinear system of time-domain ordinary differential equations is obtained. This system is solved by Newmark/Newton–Raphson techniques. The present work is based on the $\mathbf{u}-p$ formulation and the incognita fields of the coupled analysis in focus are the solid skeleton displacements and the interstitial fluid pore pressures. Independent spatial discretization is considered for each phase of the model, rendering a more flexible, efficient and robust methodology. At the end of the paper, numerical applications illustrate the accuracy and potentialities of the proposed techniques.

Keywords: Meshless Local Petrov-Galerkin, Moving Least Squares, Newmark / Newton–Raphson Method, Pore-Dynamics, Elastoplastic Analysis, Independent Phase Discretization.

1 Introduction

In spite of the great success of the finite element method and other techniques as effective numerical tools for the solution of boundary value problems on complex domains, there is still a growing interest in development of new advanced methods. Nowadays, many meshless formulations are becoming popular, due to their high adaptivity and to their low-cost effort to prepare input data (meshless methods were essentially stimulated by difficulties related to mesh generation). In addition, the need for flexibility in the selection of approximating functions (*e.g.*, the flexi-

[1] Structural Engineering Department, Federal University of Juiz de Fora, Cidade Universitária, CEP 36036-330, Juiz de Fora, MG, Brazil. Tel: +55 32 2102-3468; E-mail: delfim.soares@ufjf.edu.br

bility to use non-polynomial approximating functions) has played a significant role in the development of meshless methods. Many meshless approximations give continuous variation of the first or higher order derivatives of a primitive function in counterpart to classical polynomial approximation, where secondary fields have a jump on the interface of elements; therefore, meshless approximations are leading to more accurate results in many cases.

A variety of meshless methods has been proposed along the last decades (e.g., Belytschko *et al*., 1994; Atluri and Shen, 2002 etc.). Many of them are derived from a weak-form formulation on global domain (Belytschko *et al*., 1994) or a set of local subdomains (Atluri and Zhu, 1998; Atluri and Shen 2002; Mikhailov, 2002; Sladek *et al*. 2003, 2008). In the global formulation, background cells are required for the integration of the weak form. In methods based on local weak formulation, no cells are required (if, for the geometry of the subdomains, a simple form is chosen, numerical integrations can be easily carried out over them) and therefore they are often referred to as truly meshless methods. The meshless local Petrov-Galerkin method is a fundamental base for the derivation of many meshless formulations, since trial and test functions are chosen from different functional spaces.

Considering the analysis of porous media, most meshless formulations presented so far have been applied to analyse consolidation problems and, presently, there are only some few works concerned with pore-dynamic analysis. Considering the radial point interpolation method (RPIM), Wang and co-authors (2002, 2004, 2005) presented the numerical analysis of Biot's consolidation process, wave-induced transient response of seabeds and dissipation process of excess pore water pressure, respectively. Nogami *et al*. (2004) developed a numerical method for consolidation analysis of lumpy clay fillings by using the double porosity model and the RPIM, considering different order of interpolation functions. Wang *et al.* (2007) also presented an unequal-order radial interpolation meshless method for Biot's consolidation theory. The consolidation analysis of saturated soils with anisotropic damage and the simulation of wave motions in saturated porous media were presented by Wang *et al.* (2008) and Chen and Li (2008), respectively, taking into account the RPIM. Considering the element-free Galerkin method (EFGM), Modaressi and Aubert (1998) were among the firsts studying deforming multiphase porous media. Murakami *et al.* (2005) described a formulation for soil-water coupled problems considering finite strain analysis; Wang and Li (2006) and Wang *et al.* (2007) analysed factors influencing the solution of the consolidation problem and seabed instability, respectively; and Karim *et al*. (2002) studied the transient response of saturated porous elastic soil under cyclic loading. Some numerical issues using element-free Galerkin meshless method for coupled hydro-mechanical problems

were discussed by Oliaei *et al*. (2009). Meshless methods, based on the meshless local Petrov-Galerkin (MLPG) approach, were developed and implemented for the solution of the Biot's consolidation problem by Ferronato *et al*. (2007) and Bergamaschi (2009), taking into account axi-symmetric poroelastic models, and by Wang *et al*. (2009), taking into account plane models. The pore-dynamic analysis of elastic soils considering the MLPG was introduced by Soares (2010), taking into account Gaussian weight functions as test functions and different discretizations for each phase of the model. As far as the author is concerned, there are no publications regarding the dynamic analysis of elastoplastic porous media by MLPG formulations.

The MLPG formulation considered here adopts Heaviside step functions as test functions and employs the moving least square method to approximate the solid skeleton and the interstitial fluid incognita fields. After performing the spatial integrations, one obtains a system of nonlinear ordinary differential equations for certain nodal unknowns. That system is solved numerically by the Newmark/Newton-Raphson method. The Newmark finite difference scheme (Newmark, 1959) is applied here as a time marching technique and the Newton-Raphson method is employed as an iterative procedure to treat the nonlinear equations (as it is similarly presented by Soares *et al*., 2010, considering solid mechanics). In this work, the solid and fluid sub-domains of the porous model are analysed considering complete independent discretizations by MLPG techniques. This means that, for each phase of the model, not only different order for the interpolation functions may be considered, but also complete disassociated node distributions (as well as test and weight functions) may be adopted. This is highly important when impermeable and incompressible media are modelled, ensuring unique solvability and convergence (Soares, 2010).

2 Governing equations

The present work is focused on the $\mathbf{u}-p$ formulation, as presented by Zienkiewicz *et al*. (1984, 1990). In this case, the governing equations of the pore-dynamic model can be written as:

$$\sigma_{ij,j} - \rho_m \ddot{u}_i + \rho_m b_i = 0 \tag{1}$$

$$\alpha \dot{\varepsilon}_{ii} - (\kappa p_{,j})_{,i} + (1/Q)\dot{p} - a = 0 \tag{2}$$

where equation (1) stands for the balance of momentum of the mixture and equation (2) is a combination of the balance of mass and momentum for the interstitial fluid.

In equation (1), $\sigma_{ij}(X,t)$ is the total Cauchy stress (usual indicial notation for Cartesian axes is considered); the effective stress is defined as $\sigma'_{ij} = \sigma_{ij} + \alpha \delta_{ij} p$, where

$\alpha(X)$ accounts for slight strain changes, $p(X,t)$ stands for interstitial fluid pore-pressure and δ_{ij} represents the Kronecker delta ($\delta_{ij}=0$ if $i\neq j$ and $\delta_{ij}=1$ if $i=j$). Further on in equation (1), $u_i(X,t)$ stands for the solid matrix displacement and $b_i(X,t)$ for the body force distribution. Inferior commas and overdots indicate partial space ($u_{j,i}=\partial u_j/\partial x_i$) and time ($\dot{u}_i=\partial u_i/\partial t$) derivatives, respectively. $\rho_m=\upsilon\rho_f+(1-\upsilon)\rho_s$ stands for the mass density of the mixture, where $\rho_s(X)$ and $\rho_f(X)$ are the mass density of the solid and fluid phase, respectively, and $\upsilon(X)$ is the porosity of the medium. In equation (2), $\varepsilon_{ij}(X,t)$ represents the strain tensor and $\kappa(X)$ defines the permeability coefficients, according to the D'Arcy seepage law. $a(X,t)$ stands for domain source terms and the mixture parameter $Q(X)$ is defined by $(1/Q)=\upsilon/K_f+(\alpha-\upsilon)/K_s$, where the bulk moduli of the solid and fluid phase are represented by $K_s(X)$ and $K_f(X)$, respectively.

In equation (3) the constitutive law is written incrementally:

$$d\sigma'_{ij}=D^{ep}_{ijkl}\,d\varepsilon_{kl} \tag{3}$$

where the incremental strain components $d\varepsilon_{ij}$ are defined in the usual way (linear kinematical relations) from the displacements, i.e., $d\varepsilon_{ij}=\frac{1}{2}(du_{i,j}+du_{j,i})$. D^{ep}_{ijkl} is a tangential tensor defined by suitable state variables and the direction of the increment (nonlinear constitutive relations). Within the context of associated isotropic work hardening theory, the tangent constitutive tensor is defined as:

$$D^{ep}_{ijkl}=D_{ijkl}-(1/\psi)D_{ijmn}a_{mn}a_{op}D_{opkl} \tag{4}$$

where

$$D_{ijkl}=2\mu\nu/(1-2\nu)\,\delta_{ij}\delta_{kl}+\mu\,(\delta_{ik}\delta_{jl}+\delta_{il}\delta_{jk}) \tag{5a}$$

$$a_{kl}=\partial\bar{\sigma}/\partial\sigma'_{kl} \tag{5b}$$

$$\psi=a_{ij}D_{ijkl}a_{kl}+H \tag{5c}$$

$$H=\partial\sigma_0/\partial\bar{\varepsilon}^p \tag{5d}$$

In equations (5), $\bar{\sigma}$ and $\bar{\varepsilon}^p$ are the equivalent (or effective) stress and plastic strain, respectively; σ_0 is the uniaxial yield stress; H is the plastic-hardening modulus (the current slope of the uniaxial plastic stress-strain curve) and μ and ν stand for the shear modulus and the Poisson ratio, respectively. In case of elastic analyses, the Cauchy stresses can be defined by $\sigma'_{ij}=D_{ijkl}\varepsilon_{kl}$, where D_{ijkl} (see equation (5a)) is the elastic constitutive tensor (this linear relation is a particular case of equation (3)).

In addition to equations (1)-(5), boundary and initial conditions have to be prescribed in order to completely define the problem. They are given as follows:

(i) Boundary conditions ($t > 0$, $X \in \Gamma$ where $\Gamma = \Gamma_u \cup \Gamma_\tau = \Gamma_p \cup \Gamma_q$)

$$u_i = \bar{u}_i \text{ for } X \in \Gamma_u \tag{6a}$$

$$\tau_i = \sigma_{ij} n_j = \bar{\tau}_i \text{ for } X \in \Gamma_\tau \tag{6b}$$

$$p = \bar{p} \text{ for } X \in \Gamma_p \tag{6c}$$

$$q = p_{,j} n_j = \bar{q} \text{ for } X \in \Gamma_q \tag{6d}$$

(ii) Initial conditions ($t = 0$, $X \in \Gamma \cup \Omega$)

$$u_i = \bar{u}_{i0} \tag{7a}$$

$$\dot{u}_i = \dot{\bar{u}}_{i0} \tag{7b}$$

$$p = \bar{p}_0 \tag{7c}$$

where the prescribed values are indicated by over bars and $q(X,t)$ and $\tau_i(X,t)$ represent the fluxes and total tractions, respectively, acting along the boundary whose unit outward normal vector components are represented by $n_i(X)$. The effective tractions are defined as $\tau'_i = \tau_i + \alpha n_i p$. The domain of the model is denoted by Ω and the boundary by Γ ($\Gamma_u \cup \Gamma_\tau = \Gamma_p \cup \Gamma_q = \Gamma$ and $\Gamma_u \cap \Gamma_\tau = \Gamma_p \cap \Gamma_q = 0$).

3 Numerical discretization

In this section, the numerical discretization of the pore-dynamic model by a meshless local Petrov-Galerkin formulation is presented. First, in sub-section 3.1, the moving least square (MLS) approximation is described and, next (sub-section 3.2), the local weak-forms of the governing equations, as well as their spatial discretizations taking into account MLS approximations, are discussed. In sub-section 3.3, time-marching procedures based on the generalized Newmark method, as well as iterative procedures based on the Newton-Raphson technique, are presented, allowing the time-domain solution of the nonlinear matricial systems of equations that arise.

3.1 Moving least square approximation

In general, a meshless method uses a local approximation to represent the trial function in terms of nodal unknowns which are either the nodal values of real field variables or fictitious nodal unknowns at some randomly located nodes. The moving least squares approximation may be considered as one of such schemes, and it is employed here.

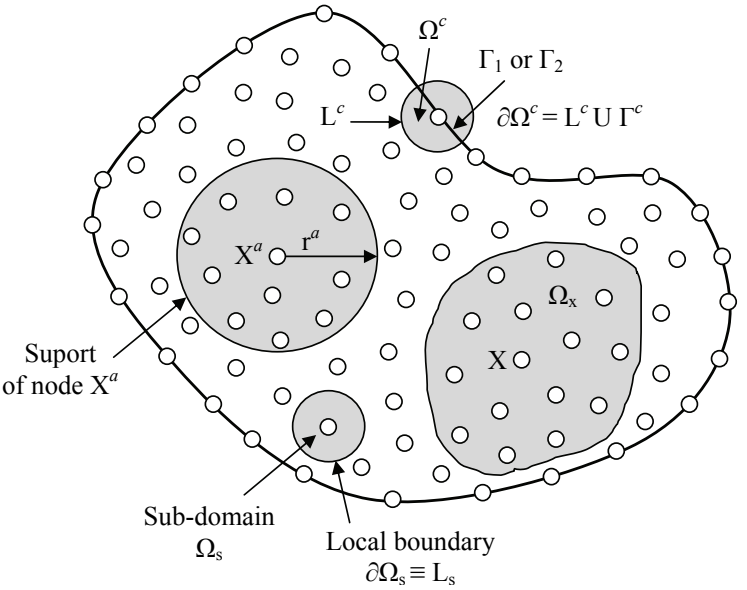

Figure 1: Local boundaries, sub-domains and domain of definition of the MLS approximation for the trial function at node X.

Consider a sub-domain Ω_x, the neighbourhood of a point X and denoted as the domain of definition of the MLS approximation for the trial function at X, which is located in the problem domain Ω (see Fig.1). Also consider a generic field φ, which represents the interstitial fluid pore-pressure field p or the solid skeleton displacement field u_i. To approximate the distribution of function φ in Ω_x, over a number of randomly located nodes, the MLS approximation of φ can be defined by (Atluri and Shen, 2002; Atluri, 2004):

$$\phi(X,t) \approx \mathbf{\Pi}^T(X)\hat{\Phi}(t) = \sum_{a=1}^{N} \eta^a(X)\hat{\phi}^a(t) \tag{8}$$

where $\hat{\phi}$ is the fictitious nodal value of ϕ and N is the number of points in the sub-domain Ω_x. The shape matrix $\mathbf{\Pi}^T(X) = \begin{bmatrix}\eta^1(X) & \eta^2(X) & \cdots & \eta^N(X)\end{bmatrix}$ is computed by:

$$\mathbf{\Pi}^T(X) = \mathbf{p}^T(X)\mathbf{A}^{-1}(X)\mathbf{B}(X) \tag{9}$$

where

$$\mathbf{A}(X) = \sum_{a=1}^{N} w^a(X)\mathbf{p}(X^a)\mathbf{p}^T(X^a) \tag{10a}$$

$$\mathbf{B}(X) = \begin{bmatrix} w^1(X)\mathbf{p}(X^1) & w^2(X)\mathbf{p}(X^2) & \cdots & w^N(X)\mathbf{p}(X^N) \end{bmatrix} \tag{10b}$$

and $\mathbf{p}^T(X) = \begin{bmatrix} p_1(X) & p_2(X) & \cdots & p_m(X) \end{bmatrix}$ is a complete monomial basis of order m. $w^a(X)$ is the weight function associated with node a. The Gaussian weight function is adopted here, and it is given by:

$$w^a(X) = \frac{\exp[-(d_a/c_a)^{2k}] - \exp[-(r_a/c_a)^{2k}]}{1-\exp[-(r_a/c_a)^{2k}]}(1-H[d_a-r_a]) \tag{11}$$

where $d_a = ||X-X^a||$ is the distance between the sampling point X and node X^a, c_a is a constant controlling the shape of the weight function and r_a is the radius of the circular support of the weight function. The Heaviside unit step function is defined as $H[z] = 1$ for $z > 0$ and $H[z] = 0$ for $z \leq 0$. The size of the weight function support should be large enough to have a sufficient number of nodes covered in the domain of definition to ensure the regularity of matrix $\mathbf{A}$.

3.2 Spatial discretization

Instead of writing the global weak-form for the governing equations described in section 2, the MLPG method constructs a weak-form over local fictitious sub-domains, such as Ω_s, which is a small region taken for each node inside the global domain (see Fig.1). The local sub-domains overlap each other, and cover the whole global domain Ω. The geometrical shape and size of local sub-domains can be arbitrary. In the present work, the local sub-domains are taken to be of circular shape. The local weak-form of the governing equations described in section 2 can be written as:

$$\int_{\partial\Omega_s} \varphi_{ik}\sigma_{ij}n_j\,d\Gamma - \int_{\Omega_s} \varphi_{ik,j}\sigma_{ij}\,d\Omega + \int_{\Omega_s} \varphi_{ik}(\rho_m b_i - \rho_m \ddot{u}_i)\,d\Omega + \beta\int_{\Gamma_{su}} \varphi_{ik}(u_i-\bar{u}_i)\,d\Gamma = 0 \tag{12a}$$

$$\int_{\partial\Omega_s} \varphi\,\kappa q\,d\Gamma - \int_{\Omega_s} \varphi_{,i}\,\kappa p_{,i} d\Omega + \int_{\Omega_s} \varphi\,(a-(1/Q)\dot{p} - \alpha\dot{\varepsilon}_{ii})\,d\Omega + \beta\int_{\Gamma_{sp}} \varphi\,(p-\bar{p})\,d\Gamma = 0 \tag{12b}$$

where φ and φ_{ik} are test functions and β is a penalty parameter, which is introduced here in order to impose essential prescribed boundary conditions in an integral form. In equations (12), $\partial\Omega_s$ is the boundary of the local sub-domain, which consists of three parts, in general: $\partial\Omega_s = L_s \cup \Gamma_{s1} \cup \Gamma_{s2}$ (see Fig.1). Here, L_s is the local boundary that is totally inside the global domain, Γ_{s2} is the part of the local

boundary which coincides with the global natural boundary, i.e., $\Gamma_{s2} = \partial\Omega_s \cap \Gamma_2$ (where Γ_2 stands for the natural boundary, i.e., $\Gamma_2 \equiv \Gamma_q$ or $\Gamma_2 \equiv \Gamma_\tau$) and, similarly, Γ_{s1} is the part of the local boundary that coincides with the global essential boundary, i.e., $\Gamma_{s1} = \partial\Omega_s \cap \Gamma_1$ (where Γ_1 stands for the essential boundary, i.e., $\Gamma_1 \equiv \Gamma_p$ or $\Gamma_1 \equiv \Gamma_u$).

In this work, plane strain problems are focused and the variables of the solid skeleton are written considering the Voigt notation (i.e., $\boldsymbol{\sigma} = \begin{bmatrix}\sigma_{11} & \sigma_{22} & \sigma_{12}\end{bmatrix}^T$, $\boldsymbol{\varepsilon} = \begin{bmatrix}\varepsilon_{11} & \varepsilon_{22} & 2\varepsilon_{12}\end{bmatrix}^T$, $\tau = \begin{bmatrix}\tau_1 & \tau_2\end{bmatrix}^T$, $\mathbf{u} = \begin{bmatrix}u_1 & u_2\end{bmatrix}^T$, $\mathbf{b} = \begin{bmatrix}b_1 & b_2\end{bmatrix}^T$ etc.). Taking into account the Voigt notation, equations (12) can be rewritten, considering the definition of effective stresses ($\sigma'_{ij} = \sigma_{ij} + \alpha\delta_{ij}p$) and expressions (8). By defining the local integral sub-domain of the meshless local Petrov-Galerkin formulation as the circle Ω^c, centred at node X^c and described by radius r_c ($\partial\Omega^c = L^c \cup \Gamma_1^c \cup \Gamma_2^c$), the expressions that arise, considering the test functions as the Heaviside step function (i.e., $\varphi = (1 - H(d_c - r_c))$ and $\varphi_{ik} = \delta_{ik}(1 - H(d_c - r_c))$), are given by:

$$\sum_{a=1}^{N}\left(\int_{\Omega^c}\rho_m\eta_u^a d\Omega\right)\ddot{\hat{\mathbf{u}}}^a - \sum_{a=1}^{N}\left(\beta\int_{\Gamma_u^c}\eta_u^a d\Gamma\right)\hat{\mathbf{u}}^a - \int_{L^c+\Gamma_u^c}\mathbf{N}\boldsymbol{\sigma}' d\Gamma + \\ + \sum_{a=1}^{N}\left(\int_{L^c+\Gamma_u^c}\mathbf{n}\alpha\eta_p^a d\Gamma\right)\hat{p}^a = \int_{\Gamma_\tau^c}\bar{\tau}\, d\Gamma + \int_{\Omega^c}\rho_m\mathbf{b}\, d\Omega - \beta\int_{\Gamma_u^c}\bar{\mathbf{u}} d\Gamma \quad (13a)$$

$$\sum_{a=1}^{N}\left(\int_{\Omega^c}(1/Q)\,\eta_p^a d\Omega\right)\dot{\hat{p}}^a - \sum_{a=1}^{N}\left(\beta\int_{\Gamma_p^c}\eta_p^a d\Gamma + \int_{L^c+\Gamma_p^c}\mathbf{n}^T\kappa\mathbf{s}_p^{aT} d\Gamma\right)\hat{p}^a + \\ + \sum_{a=1}^{N}\left(\int_{\Omega^c}\alpha\mathbf{s}_u^a d\Omega\right)\dot{\hat{\mathbf{u}}}^a = \int_{\Gamma_q^c}\kappa\bar{q}\, d\Gamma + \int_{\Omega^c} a\, d\Omega - \beta\int_{\Gamma_p^c}\bar{p} d\Gamma \quad (13b)$$

In the linear elastic case, equation (13a) simplifies to:

$$\sum_{a=1}^{N}\left(\int_{\Omega^c}\rho_m\eta_u^a d\Omega\right)\ddot{\hat{\mathbf{u}}}^a - \sum_{a=1}^{N}\left(\beta\int_{\Gamma_u^c}\eta_u^a d\Gamma + \int_{L^c+\Gamma_u^c}\mathbf{N}\mathbf{D}\mathbf{S}_u^a d\Gamma\right)\hat{\mathbf{u}}^a + \\ + \sum_{a=1}^{N}\left(\int_{L^c+\Gamma_u^c}\mathbf{n}\alpha\eta_p^a d\Gamma\right)\hat{p}^a = \int_{\Gamma_\tau^c}\bar{\tau}\, d\Gamma + \int_{\Omega^c}\rho_m\mathbf{b}\, d\Omega - \beta\int_{\Gamma_u^c}\bar{\mathbf{u}} d\Gamma \quad (14)$$

where matrices $\mathbf{N}$, $\mathbf{n}$, $\mathbf{S}^a$ and $\mathbf{s}^a$ are specified as:

$$\mathbf{N} = \begin{bmatrix} n_1 & 0 & n_2 \\ 0 & n_2 & n_1 \end{bmatrix} \tag{15a}$$

$$\mathbf{n} = \begin{bmatrix} n_1 & n_2 \end{bmatrix}^T \tag{15b}$$

$$\mathbf{S}^a = \begin{bmatrix} \eta^a_{,1} & 0 & \eta^a_{,2} \\ 0 & \eta^a_{,2} & \eta^a_{,1} \end{bmatrix}^T \tag{15c}$$

$$\mathbf{s}^a = \begin{bmatrix} \eta^a_{,1} & \eta^a_{,2} \end{bmatrix} \tag{15d}$$

and $\mathbf{D}$ is the linear elastic constitutive matrix, defined as indicated by equation (5a). In equations (13-14), subscripts u and p are relative to solid and fluid phase discretizations, respectively.

By collecting all nodal unknown fictitious values $\hat{p}^a(t)$ and $\hat{u}^a_i(t)$ into vectors $\hat{\mathbf{P}}$ and $\hat{\mathbf{U}}$, respectively, the system of the discretized equations (13) can be rewritten into matrix form as:

$$\mathbf{M}\ddot{\hat{\mathbf{U}}} + \Im(\hat{\mathbf{U}}) - \mathbf{Q}\hat{\mathbf{P}} = \mathbf{F} \tag{16a}$$

$$\mathbf{C}\dot{\hat{\mathbf{P}}} + \mathbf{H}\hat{\mathbf{P}} + \mathbf{G}\dot{\hat{\mathbf{U}}} = \mathbf{R} \tag{16b}$$

or, for the elastic linear case, equation (14) can be rewritten as:

$$\mathbf{M}\ddot{\hat{\mathbf{U}}} + \mathbf{K}\hat{\mathbf{U}} - \mathbf{Q}\hat{\mathbf{P}} = \mathbf{F} \tag{17}$$

where $\mathbf{M}$ (mass matrix) and $\mathbf{C}$ (compressibility matrix) are evaluated taking into account the first integral term on the l.h.s. of equations (14) and (13b), respectively; $\mathbf{K}$ (stiffness matrix) and $\mathbf{H}$ (permeability matrix) are computed considering the second term on the l.h.s. of equations (14) and (13b), respectively; $\mathbf{Q}$ and $\mathbf{G}$ (coupling matrices) are calculated considering the third term on the l.h.s. of equations (14) and (13b), respectively; and $\mathbf{F}$ and $\mathbf{R}$ (load nodal vectors) are evaluated considering the terms on the r.h.s. of equations (14) and (13b), respectively. In equation (16a), $\Im$ is the internal force vector, computed regarding the second and third terms on the l.h.s. of equation (13a) (for the elastic particular case, $\Im(\hat{\mathbf{U}}) = \mathbf{K}\hat{\mathbf{U}}$).

Once the ordinary differential nonlinear matrix equations (16) are established, their coupled solution in the time-domain is discussed in the next sub-section, taking into account Newmark/Newton-Raphson procedures.

It is important to note that equations (13) can be very easily implemented considering different spatial discretizations for each phase of the porous model ($\mathbf{\Pi}_p \neq \mathbf{\Pi}_u$); i.e., taking into account the present saturated porous media analysis, considering

different discretizations for the solid and fluid sub-domain (e.g., different distribution and/or number of nodes, monomial basis with different orders, different weight functions etc.). This is highly important when null permeability is considered and incompressible fluid and solid particles are analysed, in order to provide unique solvability and convergence (Soares, 2010). Even when permeable and/or compressible models are focused, different phase discretizations allow more flexible and accurate analyses, characterizing the present methodology as a more efficient and robust numerical technique (local refinements can be considered independently for each phase, coupled systems of equations of lower order can be obtained etc.). It is important to observe that, although for the MLPG it is a trivial task to consider generic independent discretizations for each phase of the model, this is a complex task for several other numerical procedures, such as the finite element method. Thus, in addition to the usually referred advantages of the MLPG, in porous media analyses, the great flexibility of the methodology to independently describe each phase of the model must be highlighted.

4 Newmark/Newton-Raphson method

For temporal discretization, the following one-step finite difference approximations are considered (generalized Newmark method):

$$\ddot{\hat{\mathbf{U}}}^{n} = (1/(\gamma_2 \Delta t^2))\, d\hat{\mathbf{U}}^{n} - (1/(\gamma_2 \Delta t))\dot{\hat{\mathbf{U}}}^{n-1} + (1 - 1/(2\gamma_2))\ddot{\hat{\mathbf{U}}}^{n-1} \tag{18a}$$

$$\dot{\hat{\mathbf{U}}}^{n} = (\gamma_1/(\gamma_2 \Delta t))\, d\hat{\mathbf{U}}^{n} + (1 - \gamma_1/\gamma_2)\dot{\hat{\mathbf{U}}}^{n-1} + \Delta t(1 - \gamma_1/(2\gamma_2))\ddot{\hat{\mathbf{U}}}^{n-1} \tag{18b}$$

$$\dot{\hat{\mathbf{P}}}^{n} = (1/(\gamma_3 \Delta t))\, d\hat{\mathbf{P}}^{n} + (1 - 1/\gamma_3)\dot{\hat{\mathbf{P}}}^{n-1} \tag{18c}$$

where Δt is the selected time-step and $\hat{\mathbf{U}}^n$ stands for a numerical approximation of $\hat{\mathbf{U}}(t_n)$ (analogously for $\hat{\mathbf{P}}^n$). For an unconditionally stable scheme, the relations $\gamma_1 \geq 0.5$, $\gamma_2 \geq 0.5\,\gamma_1$ and $\gamma_3 \geq 0.5$ must hold in equations (18), whereγ_1, γ_2 and γ_3 are the parameters of the time integration method. The temporal increment $d\hat{\mathbf{U}}^n = \hat{\mathbf{U}}^n - \hat{\mathbf{U}}^{n-1}$ is defined by the difference of values at two subsequent time instants.

Taking into account the Newmark approximations (18), equations (16) become, at a given time-instant t_n:

$$(1/(\gamma_2 \Delta t^2))\mathbf{M}\, d\hat{\mathbf{U}}^{n} + \Im(\hat{\mathbf{U}}^{n}) - \mathbf{Q}\, d\hat{\mathbf{P}}^{n} = \\ = \mathbf{F}^{n} + \mathbf{M}\,((1/(\gamma_2 \Delta t))\dot{\hat{\mathbf{U}}}^{n-1} + (1/(2\gamma_2) - 1)\ddot{\hat{\mathbf{U}}}^{n-1}) + \mathbf{Q}\hat{\mathbf{P}}^{n-1} \tag{19a}$$

$$(\gamma_1/(\gamma_2\Delta t))\mathbf{G}\,d\hat{\mathbf{U}}^n + ((1/(\gamma_3\Delta t))\mathbf{C}+\mathbf{H})\,d\hat{\mathbf{P}}^n = \mathbf{R}^n + \\ +\mathbf{C}((1/\gamma_3-1)\dot{\hat{\mathbf{P}}}^{n-1}) + \mathbf{G}((\gamma_1/\gamma_2-1)\dot{\hat{\mathbf{U}}}^{n-1} + \Delta t(\gamma_1/(2\gamma_2)-1)\ddot{\hat{\mathbf{U}}}^{n-1}) - \mathbf{H}\hat{\mathbf{P}}^{n-1} \tag{19b}$$

Due to the nonlinearities involved in the internal force vector, each increment $d\hat{\mathbf{U}}^n$ must be computed iteratively, taking into account the incremental constitutive law (3). Let the iterative variation be defined independently of the time instant as $\delta\hat{\mathbf{U}}_{(k+1)} = \hat{\mathbf{U}}^n_{(k+1)} - \hat{\mathbf{U}}^n_{(k)}$ (analogously for $\delta\hat{\mathbf{P}}_{(k+1)}$). Then $d\hat{\mathbf{U}}^n_{(k+1)} = d\hat{\mathbf{U}}^n_{(k)} + \delta\hat{\mathbf{U}}_{(k+1)}$, and consideration of equations (19) at the $(k+1)^{st}$ iterative step yields the following system of nonlinear algebraic equations:

$$(1/(\gamma_2\Delta t^2))\mathbf{M}\,\delta\hat{\mathbf{U}}_{(k+1)} + \Im(\hat{\mathbf{U}}^n_{(k)} + \delta\hat{\mathbf{U}}_{(k+1)}) - \mathbf{Q}\delta\hat{\mathbf{P}}_{(k+1)} = \\ = \mathbf{F}^n + \mathbf{M}(-(1/(\gamma_2\Delta t^2))\,d\hat{\mathbf{U}}^n_{(k)} + (1/(\gamma_2\Delta t))\dot{\hat{\mathbf{U}}}^{n-1} + (1/(2\gamma_2)-1)\ddot{\hat{\mathbf{U}}}^{n-1}) + \\ + \mathbf{Q}(\hat{\mathbf{P}}^{n-1} + d\hat{\mathbf{P}}^n_{(k)}) \tag{20a}$$

$$(\gamma_1/(\gamma_2\Delta t))\mathbf{G}\,\delta\hat{\mathbf{U}}_{(k+1)} + ((1/(\gamma_3\Delta t))\mathbf{C}+\mathbf{H})\,\delta\hat{\mathbf{P}}_{(k+1)} = \\ = \mathbf{R}^n + \mathbf{C}(-(1/(\gamma_3\Delta t))d\hat{\mathbf{P}}^n_{(k)} + (1/\gamma_3-1)\dot{\hat{\mathbf{P}}}^{n-1}) + \mathbf{G}(-(\gamma_1/(\gamma_2\Delta t))d\hat{\mathbf{u}}^n_{(k)} + \\ + (\gamma_1/\gamma_2-1)\dot{\hat{\mathbf{U}}}^{n-1} + \Delta t(\gamma_1/(2\gamma_2)-1)\ddot{\hat{\mathbf{U}}}^{n-1}) - \mathbf{H}(\hat{\mathbf{P}}^{n-1} + d\hat{\mathbf{P}}^n_{(k)}) \tag{20b}$$

Making use of the linearization of the nonlinear term $\Im(\hat{\mathbf{U}}^n_{(k)} + \delta\hat{\mathbf{U}}_{(k+1)})$ with respect to the iterative variation $\delta\hat{\mathbf{U}}_{(k+1)}$, one obtains in view of equations (13a) and (16a):

$$\Im^c(\hat{\mathbf{U}}^n_{(k)} + \delta\hat{\mathbf{U}}_{(k+1)}) = \\ = -\sum_{a=1}^{N}\left(\beta\int_{\Gamma^c_u}\eta^a_u d\Gamma\right)(\hat{\mathbf{u}}^{a\,n}_{(k)} + \delta\hat{\mathbf{u}}^a_{(k+1)}) - \int_{L^c+\Gamma^c_u}\mathbf{N}(\boldsymbol{\sigma}'^n_{(k)} + \delta\boldsymbol{\sigma}'_{(k+1)})d\Gamma = \\ = \Im^c(\hat{\mathbf{U}}^n_{(k)}) - \sum_{a=1}^{N}\left(\beta\int_{\Gamma^c_u}\eta^a_u d\Gamma + \int_{L^c+\Gamma^c_u}\mathbf{N}\mathbf{D}^{ep}_{(k)}\mathbf{S}^a_u d\Gamma\right)\delta\hat{\mathbf{u}}^a_{(k+1)} = \\ = \Im^c(\hat{\mathbf{U}}^n_{(k)}) + \mathbf{K}^c_T(\hat{\mathbf{U}}^n_{(k)})\delta\hat{\mathbf{U}}_{(k+1)} \tag{21}$$

where $\mathbf{K}_T$ is the tangent stiffness matrix, with sub-matrices given by:

$$\mathbf{K}^{ca}_T(\hat{\mathbf{U}}^n_{(k)}) = \frac{\partial\Im^c(\hat{\mathbf{U}}^n_{(k)})}{\partial\hat{\mathbf{u}}^a} = -\beta\mathbf{I}\int_{\Gamma^c_u}\eta^a_u d\Gamma - \int_{L^c+\Gamma^c_u}\mathbf{N}\mathbf{D}^{ep}_{(k)}\mathbf{S}^a_u d\Gamma \tag{22}$$

In equation (22), $\mathbf{I}$ stands for the identity matrix and $\mathbf{D}^{ep}_{(k)}(\hat{\mathbf{U}}^n_{(k)})$ is computed according to definitions (3)-(5) in Voigt notation, i.e., $\boldsymbol{\sigma}'^n_{(k)} = \boldsymbol{\sigma}'^{n-1} + d\boldsymbol{\sigma}'^n_{(k)} = \boldsymbol{\sigma}'^{n-1} + \mathbf{D}^{ep}_{(k)} d\boldsymbol{\varepsilon}^n_{(k)}$ etc. If the initial stress formulation is considered (which is an appropriate technique for dynamic analysis), the tangent stiffness matrix is never updated, and $\mathbf{K}_T = \mathbf{K}$ is assumed.

Finally, in view of equations (21)-(22), equations (20) become:

$$\begin{bmatrix} (1/(\gamma_2\Delta t^2))\mathbf{M} + \mathbf{K}_T & -\mathbf{Q} \\ (\gamma_1/(\gamma_2\Delta t))\mathbf{G} & (1/(\gamma_3\Delta t))\mathbf{C} + \mathbf{H} \end{bmatrix} \begin{bmatrix} \delta\hat{\mathbf{U}}_{(k+1)} \\ \delta\hat{\mathbf{P}}_{(k+1)} \end{bmatrix} = \begin{bmatrix} \bar{\mathbf{F}}^n_{(k)} \\ \bar{\mathbf{R}}^n_{(k)} \end{bmatrix} \tag{23}$$

where its r.h.s. is defined by:

$$\bar{\mathbf{F}}^n_{(k)} = \mathbf{F}^n - \Im(\hat{\mathbf{U}}^n_{(k)}) + \mathbf{M}\left(-(1/(\gamma_2\Delta t^2))\, d\hat{\mathbf{U}}^n_{(k)} + (1/(\gamma_2\Delta t))\dot{\hat{\mathbf{U}}}^{n-1} + \right.$$
$$\left. + (1/(2\gamma_2) - 1)\ddot{\hat{\mathbf{U}}}^{n-1}\right) + \mathbf{Q}(\hat{\mathbf{P}}^{n-1} + d\hat{\mathbf{P}}^n_{(k)}) \tag{24a}$$

$$\bar{\mathbf{R}}^n_{(k)} = \mathbf{R}^n + \mathbf{C}\left(-(1/(\gamma_3\Delta t))d\hat{\mathbf{P}}^n_{(k)} + (1/\gamma_3 - 1)\dot{\hat{\mathbf{P}}}^{n-1}\right) + \mathbf{G}\left(-(\gamma_1/(\gamma_2\Delta t))d\hat{\mathbf{U}}^n_{(k)} + \right.$$
$$\left. + (\gamma_1/\gamma_2 - 1)\dot{\hat{\mathbf{U}}}^{n-1} + \Delta t(\gamma_1/(2\gamma_2) - 1)\ddot{\hat{\mathbf{U}}}^{n-1}\right) - \mathbf{H}(\hat{\mathbf{P}}^{n-1} + d\hat{\mathbf{P}}^n_{(k)}) \tag{24b}$$

Equations (23)-(24) enable the computation of the solid skeleton displacements and of the interstitial fluid pore-pressures at each iterative step, of each time step (one should keep in mind that $\hat{\mathbf{U}}^n_{(k+1)} = \hat{\mathbf{U}}^n_{(k)} + \delta\hat{\mathbf{U}}_{(k+1)}$; $d\hat{\mathbf{U}}^n_{(k+1)} = d\hat{\mathbf{U}}^n_{(k)} + \delta\hat{\mathbf{U}}_{(k+1)}$ etc.).

5 Numerical aspects and applications

Two numerical applications are considered here, illustrating the discussed methodologies. In the first application, the simulation of a linear one-dimensional problem is focused, and a soil column is analysed taking into account different material properties. In the second application, a nonlinear two-dimensional soil strip is considered. The results obtained by the proposed MLPG formulation are compared with analytical answers, whenever possible, and with results provided by the Finite Element Method (FEM).

In the present work, the radii of the influence domain and of the local sub-domain are set to $\theta_x d_i^3$ and $\theta_s d_i^1$, respectively; where d_i^3 and d_i^1 are the distances to the third and first nearest points from node i, respectively. In all the applications that follow, $\theta_x = 4.0$ and $\theta_s = 0.6$ are adopted. Complete monomial bases of order $m = 6$ are considered. The time-integration parameters are selected regarding the trapezoidal

rule, i.e.: $\gamma_1 = 0.5$, $\gamma_2 = 0.25$ and $\gamma_3 = 0.5$, and the mass and compressibility matrices are diagonalized by a row-sum technique. Regarding the iterative process, convergence is achieved once the relative norm of the results computed by equation (23) is smaller than a given tolerance and, for all the applications that follow, a tight tolerance of 10^{-5} is selected. In the present work, the tangent stiffness matrix is never updated along the nonlinear analysis (initial stress formulation) and it can be considered as the linear stiffness matrix expressed in equation (17).

5.1 Linear analysis

In this first example, a soil column is analysed (de Boer *et al.*, 1993; Diebels and Ehlers, 1996; Schanz and Cheng, 2000; Soares *et al.*, 2006; Soares, 2008 and 2010). A sketch of the model is depicted in Fig.2. The top surface of the column is considered drained and uniformly loaded. The other surfaces of the model are undrained and have null normal displacements prescribed. 561 nodes are employed to spatially discretize the rectangular domain ($H = 10m$).

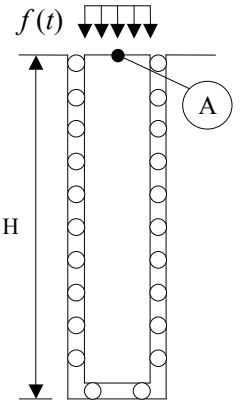

Figure 2: Sketch of the soil column model.

Two kinds of soils and load amplitudes are considered here (the loads have a Heaviside time variation). The properties of the models are specified below:

Model 1 – for the present model, the load amplitude is 3 kN/m^2. The physical properties of the soil are: $\nu = 0.3$ (Poisson); $E = 14515880N/m^2$ (Young Modulus); $\rho_s = 2000kg/m^3$ (mass density – solid phase); $\rho_f = 1000kg/m^3$ (mass density – fluid phase); $\upsilon = 0.33$ (porosity); $\kappa = 10^{-6}m^4/Ns$ (permeability). The soil is incompressible and the time discretization considered is given by $\Delta t = 10^{-3}s$;

Model 2 – for the present model, the load amplitude is 1 kN/m^2. The physical properties of the soil are: $\nu = 0.298$; $E = 254423076.9N/m^2$; $\rho_s = 2700kg/m^3$;

$\rho_f = 1000 kg/m^3$; $\upsilon = 0.48$; $\kappa = 3.55 \cdot 10^{-9} m^4/Ns$. The soil is compressible and $K_s = 1.1 \cdot 10^{10} N/m^2$ (compression modulus – solid phase); $K_f = 3.3 \cdot 10^9 N/m^2$ (compression modulus – fluid phase). The time-step is $\Delta t = 10^{-4} s$.

In Fig.3, vertical displacements at point A are depicted, taking into account Model 1 and Model 2. As can be observed in Fig.3(a), the results obtained by the MLPG formulation are in good agreement with the analytical results provided by de Boer *et al.* (1993) and with the results provided by the FEM. In Fig.3(b), once again, the MLPG results are in good agreement with the results provided by the semi-analytical procedures presented by Dubner and Abate (1968) and Schanz and Cheng (2000) and with those provided by the FEM.

5.2 Nonlinear analysis

In this second example, a two-dimensional soil strip is analysed (Li *et al.*, 2003; Soares *et al.*, 2006; Soares, 2008 and 2010). A sketch of the model is depicted in Fig.4. The geometry of the strip is defined by $a = 5\,m$, $b = 10\,m$ and $c = 1\,m$. The symmetry of the model is taken into account and two possibilities are considered for the solid and fluid phase discretizations, namely: (i) Discretization 1 – 441 nodes are employed to spatially discretize the solid and the fluid phases; (ii) Discretization 2 – 441 nodes are employed to spatially discretize the solid phase and 121 nodes are employed to spatially discretize the fluid phase.

The soil strip is loaded as indicted in Fig.4 (in kN/m^2) and the adopted time-step is $\Delta t = 5 \cdot 10^{-4} s$. The soil is compressible (fluid phase) and permeable: $\nu = 0.2$; $E = 10^7 N/m^2$; $\rho_s = 2538.5 kg/m^3$; $\rho_f = 1000 kg/m^3$; $\upsilon = 0.35$; $\kappa = 10^{-7} m^4/Ns$ and $K_f = 3.3 \cdot 10^9 N/m^2$. A perfectly plastic material obeying the Mohr-Coulomb yield criterion is assumed, where $c = 2 \cdot 10^2 N/m^2$ (cohesion) and $\theta = 10^0$ (internal friction angle).

Vertical displacements at point A (see Fig.4) are depicted in Fig.5, considering discretizations 1 and 2, and linear and nonlinear analyses. As can be observed, the results provided by the proposed MLPG formulation are in good agreement with those provided by the FEM. Discretization 2 is a very appropriate discretization for the model (and for pore-mechanic analyses, in general): not only it renders a smaller system of coupled equations (providing more efficient analyses) than discretization 1, maintaining the good accuracy of the results, but also it allows the numerical simulation of impermeable and incompressible media, as is described in Figs.6 and 7.

Fig.6 depicts the pore-pressure distributions along the modelled soil strip at time $t = 1.0s$, considering the soil as impermeable and incompressible (i.e., $\kappa = 0$ and $K_s = K_f = \infty$) and the two discretizations in focus. As can be observed, discretiza-

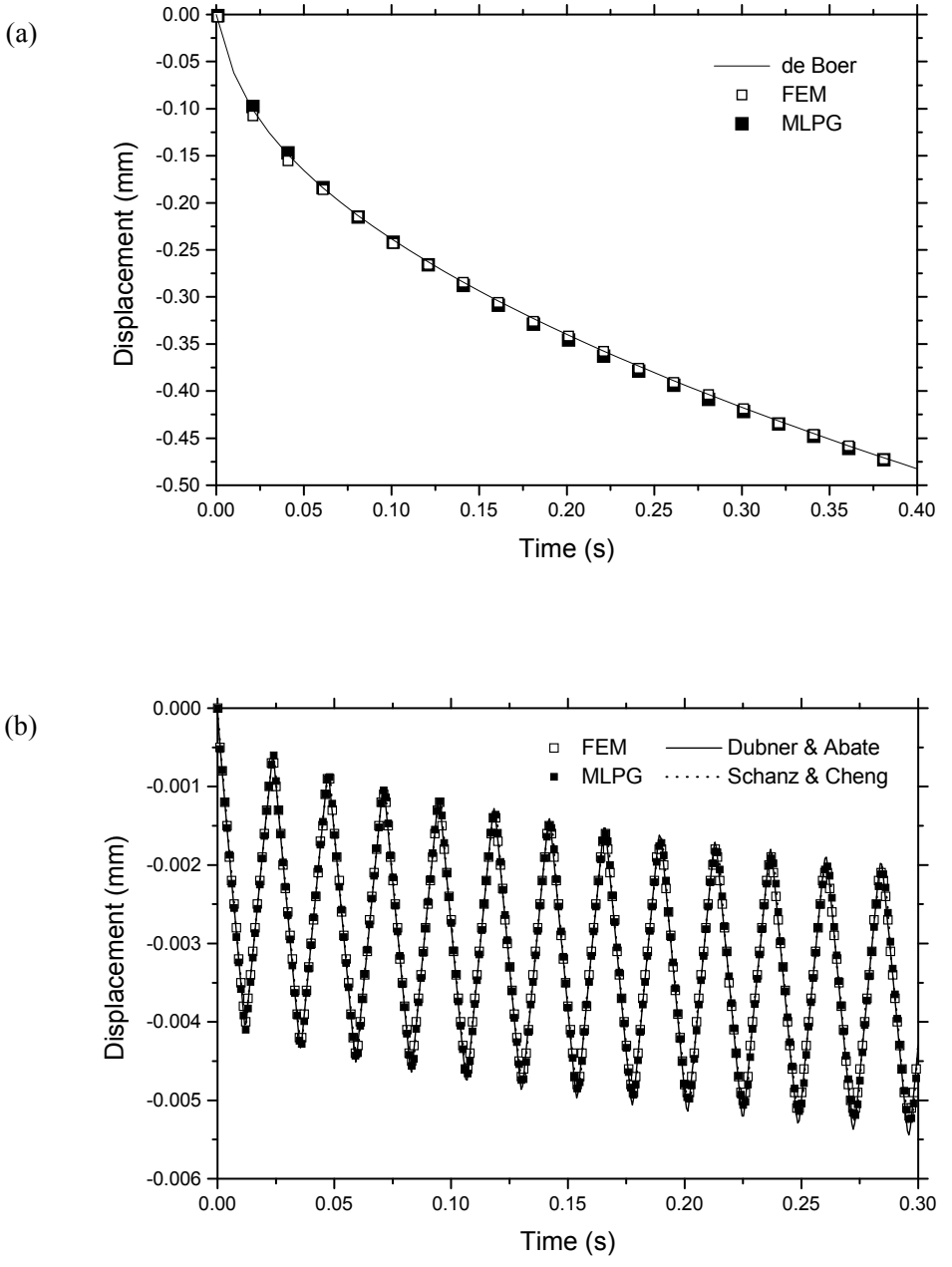

Figure 3: Displacements at point A for the (a) incompressible (Model 1) and (b) compressible (Model 2) soil column.

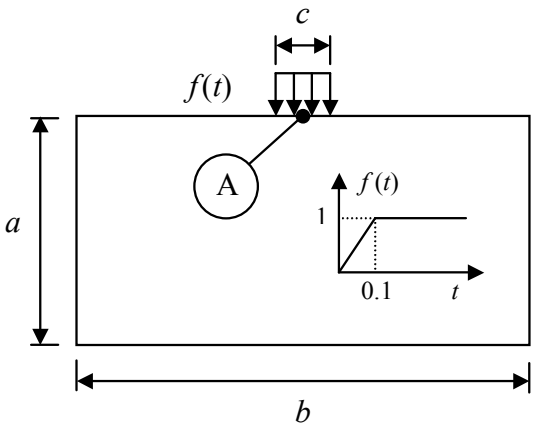

Figure 4: Sketch of the soil strip model.

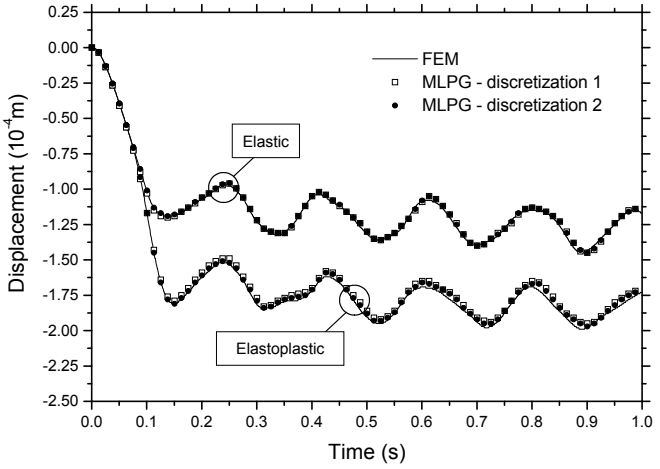

Figure 5: Displacements at point A for the compressible and permeable soil strip considering linear and nonlinear analyses.

tion 1 do not fulfil the solvability condition, providing unstable results (in a finite element context, for instance, in the limit of zero compressibility of water and soil grains and zero permeability, the functions used to interpolate displacements and pressures must fulfil either the Babuska-Brezzi conditions – Babuska, 1973; Brezzi, 1974 – or the simpler patch test proposed by Zienkiewicz *et al.*, 1986: these requirements exclude the use of elements with equal order interpolation for pressures and displacements, for which spurious oscillations may appear). Discretization 2, on

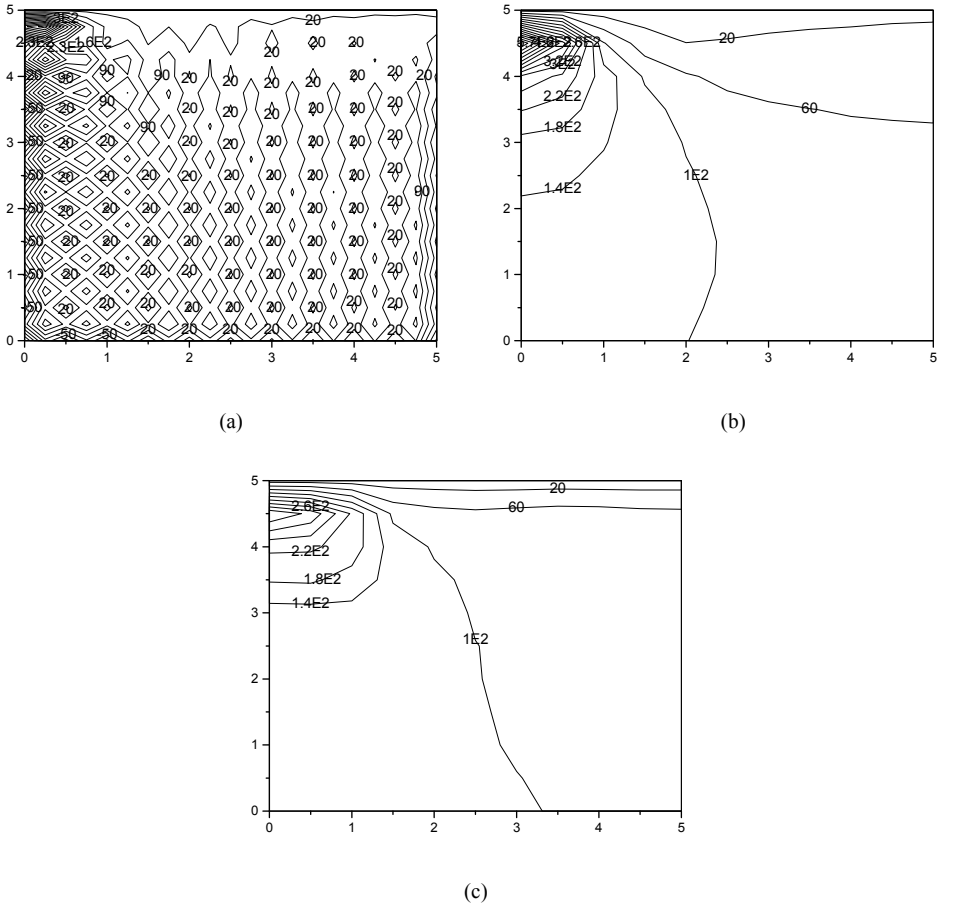

Figure 6: Pore-pressure field for the impermeable and incompressible soil strip at time $t = 1.0s$ considering: (a) discretization 1 (linear analysis); (b) discretization 2 (linear analysis); (c) discretization 2 (nonlinear analysis).

the other hand, allows an appropriate numerical simulation of the model, and the results depicted in Fig.6(b) are in good agreement with other authors/methodologies results (see, for instance, Li *et al*., 2003; Soares, 2010, etc.).

Vertical displacements at point A are depicted in Fig.7, considering the soil as impermeable and incompressible (discretization 2), and linear and nonlinear analyses.

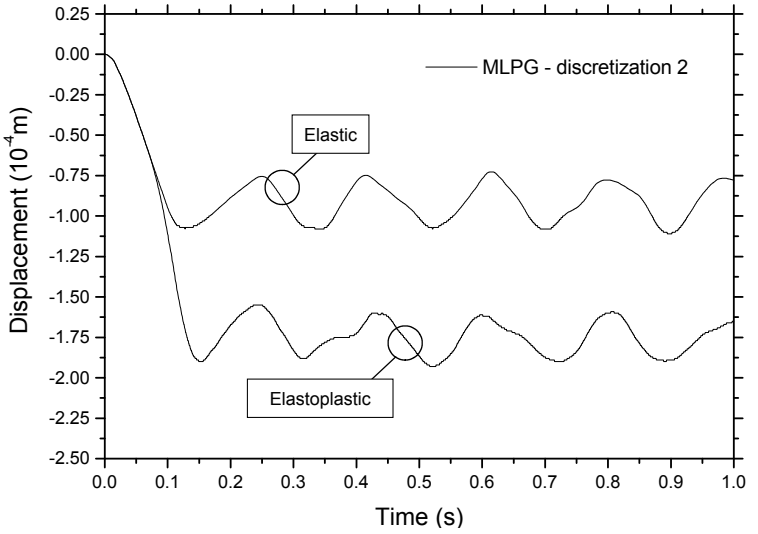

Figure 7: Displacements at point A for the incompressible and impermeable soil strip considering linear and nonlinear analyses.

6 Conclusions

In this work, time-domain dynamic analyses of nonlinear porous media, taking into account MLPG formulations, are discussed. In the present MLPG approach, Heaviside step functions are adopted as test functions (eliminating some domain integrals of the local weak form equations) and a MLS interpolation scheme is considered (independently for each phase of the model), rendering a nonlinear time-domain matricial system of coupled equations. This system is analysed by iterative time-marching procedures based on Newmak/Newton-Raphson techniques. Numerical results are presented at the end of the paper, illustrating the good accuracy, stability and flexibility of the proposed methodologies.

The adoption of different spatial discretizations for each phase of the porous model is very important. Not only it may provide more accurate, efficient and flexible simulations, but also it permits the analysis of impermeable and incompressible media. It must be highlighted that the introduction of independent phase discretization by meshless local Petrov-Galerkin techniques is much easier to implement than in mesh-based formulations, such as the finite element method. In the present work a very generic methodology is discussed, allowing a complete independency of the solid and fluid phase discretizations (in fact, analyses can be carried out here without a single common node for both phases).

It is also important to highlight that the adopted meshless technique gives continuous variation of the first (or higher order) derivatives of the primitive function (in counterpart to classical FEM polynomial approximations where secondary fields have a jump on the interface of elements) and, therefore, more accurate results are expected in elastoplastic analyses by these techniques, since proper computation of stresses plays a crucial role on these nonlinear models. Moreover, for these models, MLPG formulations based on Heaviside step functions as test functions are considerably more efficient than other MLPG formulations (such as those based on Gaussian weight function as the test functions, for instance), since the stress states of the model are computed just for a small number of integration points (only local boundary integrations are necessary – see equation (13a)), allowing an efficient evaluation of the internal forces. MLPG formulations based on Heaviside step functions also seem to deal better with the spurious modes related to the dynamic analysis (Soares *et al*, 2009), allowing more stable numerical procedures when considering the Newmark time-marching scheme.

Acknowledgement: The financial support by CNPq (*Conselho Nacional de Desenvolvimento Científico e Tecnológico*) and FAPEMIG (*Fundação de Amparo à Pesquisa do Estado de Minas Gerais*) is greatly acknowledged.

References

Atluri, S.N. (2004): *The Meshless Method (MLPG) for Domain & BIE Discretizations*, Tech Science Press, Encino, CA.

Atluri, S.N., Shen, S. (2002): *The Meshless Local Petrov-Galerkin (MLPG) Method*, Tech Science Press, Encino, CA.

Atluri, S.N., Shen, S.P. (2002): The meshless local Petrov-Galerkin (MLPG) method: A simple & less costly alternative to the finite element and boundary element methods, *CMES: Computer Modeling in Engineering & Sciences* vol.3, pp. 11-51.

Atluri, S.N., Zhu, T. (1998): A New Meshless Local Petrov-Galerkin (MLPG) Approach in Computational Mechanics, *Computational Mechanics* vol.22, pp. 117-127.

Babuska, I. (1973): The finite element method with Lagrange multiplier, *Numerische Mathematik* vol.20, pp. 179-192.

Belytschko, T., Lu, Y., Gu, L. (1994): Element free Galerkin methods, *International Journal for Numerical Methods in Engineering* vol.37, pp. 229-256.

Bergamaschi, L. (2009): An Efficient Parallel MLPG Method for Poroelastic Models, *CMES: Computer Modeling in Engineering & Sciences* vol.29, pp. 191-

215.

Brezzi, F. (1974): On the existence, uniqueness and approximation of saddle point problems arising from Lagragian multipliers, *RAIRO 8-R2*, pp. 129-151.

Chen, S.L., Li, Y.X. (2008): An efficient RPIM for simulating wave motions in saturated porous media. *International Journal of Solids and Structures* vol.45, pp. 6316-6332.

de Boer, R., Ehlers, W., Liu, Z. (1993): One-dimensional transient wave propagation in fluid saturated incompressible porous media, *Archive of Applied Mechanics* vol.63, pp. 59-72.

Diebels, S., Ehlers, W. (1996): Dynamic analysis of a fully saturated porous medium accounting for geometrical and material non-linearities. *International Journal for Numerical Methods in Engineering* vol.49, pp. 833-848.

Dubner, H., Abate, J. (1968): Numerical inversion of Laplace transforms by relating them to the finite Fourier cosine transform, *Journal of the Association for Computing Machinery* vol.15, pp. 115-123.

Ferronato, M., Mazzia, A., Pini, G., Gambolati, G. (2007): A meshless method for axi-symmetric poroelastic simulations: Numerical study, *International Journal for Numerical Methods in Engineering* vol.70, pp. 1346-1365.

Karim, M.R. Nogami, T. Wang, J.G. (2002): Analysis of transient response of saturated porous elastic soil under cyclic loading using element-free Galerkin method, *International Journal of Solids and Structures* vol.39, pp. 6011-6033.

Li, X., Han, X., Pastor, M. (2003): An iterative stabilized fractional step algorithm for finite element analysis in saturated soil dynamics, *Computational Methods in Applied Mechanics and Engineering* vol.192, pp. 3845-3859.

Mikhailov, S.E. (2002): Localized boundary-domain integral formulations for problems with variable coefficients, *Engineering Analysis with Boundary Elements* vol.26, pp. 681-690.

Modaressi, H., Aubert, P. (1998): Element-free Galerkin method for deforming multiphase porous media, *International Journal for Numerical Methods in Engineering* vol.42, pp. 313-340.

Murakami, A., Setsuyasu, T., Arimoto, S. (2005): Mesh-free method for soil-water coupled problem within finite strain and its numerical validity, *Soils and Foundations* vol.45, pp. 145-154.

Newmark, N.M. (1959): A method of computation for structural dynamics, *ASCE Journal of Engineering Mechanics Division* vol.85, pp. 67-94.

Nogami, T., Wang, W., Wang, J.G. (2004): Numerical method for consolidation analysis of lumpy clay fillings with meshless method, *Soils and Foundations* vol.44,

pp. 125-142.

Oliaei, M.N. (2009): Some numerical issues using element-free Galerkin meshless method for coupled hydro-mechanical problems, *International Journal for Numerical and Analytical Methods in Geomechanics* vol.33, pp. 915-938.

Schanz, M., Cheng, A.H.D. (2000): Transient wave propagation in a one-dimensional poroelastic column, *Acta Mechanica* vol.145, pp. 1-18.

Sladek, J.; Sladek, V.; Zhang, C.Z. (2003): Application of meshless local Petrov-Galerkin (MLPG) method to elastodynamic problems in continuously nonhomogeneous solids, *CMES: Computer Modeling in Engineering & Sciences* vol.4, pp. 637-647.

Sladek, J.; Sladek, V.; Zhang, C.H. (2008): Computation of stresses in nonhomogeneous elastic solids by local integral equation method: a comparative study, *Computational Mechanics* vol.41, pp. 827-845.

Soares Jr., D. (2008): A time-domain FEM approach based on implicit Green's functions for the dynamic analysis of porous media, *Computational Methods in Applied Mechanics and Engineering* vol.197, pp. 4645–4652.

Soares Jr., D. (2010): Dynamic Analysis of Porous Media Considering Unequal Phase Discretization by Meshless Local Petrov-Galerkin Formulations, *CMES: Computer Modeling in Engineering & Sciences* vol.61, pp. 177–200.

Soares Jr., D., Sladek, J., Sladek, V. (2009): Time-domain analysis of elastodynamic models discretized by meshless local Petrov-Galerkin formulations, Advances in Boundary Element Techniques X vol.3, pp. 375–380.

Soares Jr., D., Sladek, J., Sladek, V. (2010): Nonlinear dynamic analyses by meshless local Petrov-Galerkin formulations, *International Journal for Numerical Methods in Engineering* vol.81, pp. 1687–1699.

Soares Jr., D., Telles, J.C.F., Mansur, W.J. (2006): A time-domain boundary element formulation for the dynamic analysis of non-linear porous media, *Engineering Analysis with Boundary Elements* vol.30, pp. 363-370.

Wang, J.G., Karim, M.R., Lin, P.Z. (2007): Analysis of seabed instability using element free Galerkin method, *Ocean Engineering* vol.34, pp. 247-260.

Wang, J.G., Liu, G.R., Lin, P. (2002): Numerical analysis of Biot's consolidation process by radial point interpolation method, *International Journal of Solids and Structures* vol.39, pp. 1557-1573.

Wang, J.G., Xie, H., Leung, C.F. (2009): A local boundary integral-based meshless method for Biot's consolidation problem, *Engineering Analysis with Boundary Elements* vol.33, pp. 35-42.

Wang, J.G., Yan, L., Liu, G.R. (2005): A local radial point interpolation method

for dissipation process of excess pore water pressure, *International Journal of Numerical Methods for Heat & Fluid Flow* vol.15, pp. 567–587.

Wang, J.G., Zhang, B.Y., Nogami, T. (2004): Wave-induced seabed response analysis by radial point interpolation meshless method, *Ocean Engineering* vol.31, pp. 21-42.

Wang, W.D., Wang, J.G., Wang, Z.L., Nogami, T. (2007): An unequal-order radial interpolation meshless method for Biot's consolidation theory, *Computers and Geotechnics* vol.34, pp. 61-70.

Wang, Z.L., Li, Y.C. (2006): Analysis of factors influencing the solution of the consolidation problem by using an element-free Galerkin method, *Computers & Geosciences* vol.32, pp. 624-631.

Wang, Z.L., Wang, J.G., Shen, R.F. (2008): The application of a meshless method to consolidation analysis of saturated soils with anisotropic damage, *Computers & Geosciences* vol.34, pp. 849-859.

Zienkiewicz, O.C., Chan, A.H.C., Pastor, M., Paul, D.K., Shiomi, T (1990): Static and dynamic behavior of soils: a rational approach to quantitative solutions. I. Fully saturated problems, *Proceedings of the Royal Society of London* vol.429, pp. 285-309.

Zienkiewicz, O.C., Qu, S., Taylor, R.L., Nakzawa, S. (1986): The patch test for mixed formulation, *International Journal for Numerical Methods in Engineering* vol.23, pp. 1871-1883.

Zienkiewicz, O.C., Shiomi, T. (1984): Dynamic behavior of saturated porous media: the generalized Biot formulation and its numerical solution, *International Journal for Numerical and Analytical Methods in Geomechanics* vol.8, pp. 71-96.